

# LSDAT: Low-Rank and Sparse Decomposition for Decision-based Adversarial Attack

Ashkan Esmaeili<sup>1\*</sup>, Marzieh Edraki<sup>1\*</sup>, Nazanin Rahnavard<sup>\*</sup>, Mubarak Shah<sup>†</sup>, Ajmal Mian<sup>‡</sup>

<sup>\*</sup> University of Central Florida <sup>†</sup> Center for Research in Computer Vision <sup>‡</sup> University of Western Australia

ashkan.esmaeili@ucf.edu

1 indicates shared first authorship

**Abstract**—We propose LSDAT, an image-agnostic decision-based black-box attack that exploits low-rank and sparse decomposition (LSD) to dramatically reduce the number of queries and achieve superior fooling rates compared to the state-of-the-art decision-based methods under given imperceptibility constraints. LSDAT crafts perturbations in the low-dimensional subspace formed by the sparse component of the input sample and that of an adversarial sample to obtain query-efficiency. The specific perturbation of interest is obtained by traversing the path between the input and adversarial sparse components. It is set forth that the proposed sparse perturbation is the most aligned sparse perturbation with the shortest path from the input sample to the decision boundary for some initial adversarial sample (the best sparse approximation of shortest path, likely to fool the model). Theoretical analyses are provided to justify the functionality of LSDAT. Unlike other dimensionality reduction based techniques aimed at improving query efficiency (e.g, ones based on FFT), LSD works directly in the image pixel domain to guarantee that non- $l_2$  constraints, such as sparsity, are satisfied. LSD offers better control over the number of queries and provides computational efficiency as it performs sparse decomposition of the input and adversarial images only once to generate all queries. We demonstrate  $l_0$ ,  $l_2$  and  $l_\infty$  bounded attacks with LSDAT to evince its efficiency compared to baseline decision-based attacks in diverse low-query budget scenarios as outlined in the experiments.<sup>1</sup>

## I. INTRODUCTION

Deep neural networks (DNN) have been employed to yield high accuracy in many image classification related tasks [47]. However, despite their high accuracy, the possibility of adversarial attacks has cast a shadow over the versatility of deep learning models. This vulnerability to adversarial attacks can lead to catastrophic consequences in applications which are safety-critical such as autonomous driving, malware detection, spam detection, intrusion detection, cybersecurity, video surveillance, robotics, and financial services fraud detection [53]. Adversarial attacks are applicable to all deep learning based real-world systems such as speech recognition [11], speech-to-text conversion [13], face recognition [48], visual classification [24], malware detection [30], [27], and other general physical world cases as discussed in [34], [4]. In this paper, we focus on the image-classification task. Adversarial attacks are mainly studied to gain insights into the inner working of DNNs or to measure their robustness. Adversarial attacks can be launched in a white-box setting, where access to the complete DNN model is available [26], [41], [12], [38],

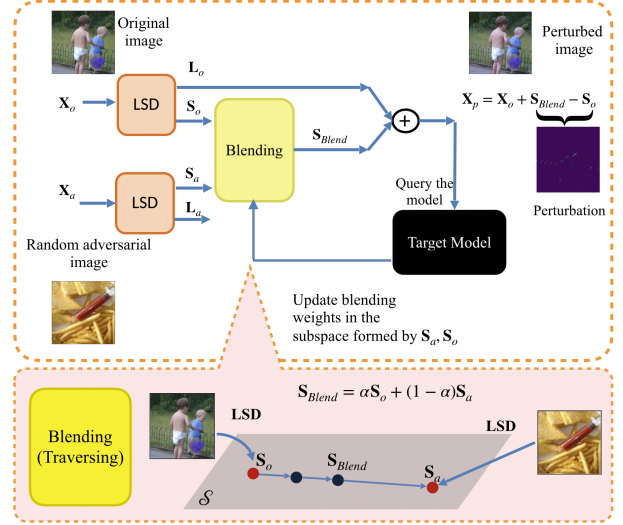


Fig. 1: LSDAT. First, low-rank and sparse decomposition is performed to extract sparse components of the input image and a random initial adversarial sample. The sparse components constitute a low-dimensional subspace ( $\mathcal{S}$ ) in the image space. Then, the attacker gradually traverses the path between the two sparse components with a pre-determined step size ( $\alpha$ ) and blends the sparse components via a weighted combination. The perturbed image can be obtained by adding the result of blended sparse components to the low-rank component of the input image. The target model is queried with the perturbed image. This iterative process continues until the model is fooled or the query budget gets exhausted.

[45], [33], as well as in a black-box setting, where access to only the model output is available [1]. In the latter case, the DNN model is queried with samples and the outputs are analyzed to optimize the attack. It is critical for adversarial attacks to perform efficiently and with a low-query budget because large number of queries entail computational complexity and can make the target network skeptical of an unusual activity. To this end, we propose Low-Rank and Sparse Decomposition (LSD) for decision based black-box attack; LSDAT for brevity, which is efficient and works under a very low-query budget. The main contributions of LSDAT are summarized as follows:

- We propose an efficient decision-based black-box attack exploiting the low rank and sparse decomposition (LSD) of images to craft sparse adversarial perturbation in a sparse domain. We show that crafting the perturbation in this low-dimensional subspace of sparse representations reduces queries and leads to computationally more efficient attack compared to other dimensionality reduction techniques.

<sup>1</sup>LSDAT implementation will be made public.

- We provide theoretical analyses showing the proposed perturbation direction is highly likely the most aligned sparse perturbation with the shortest path from the original image to the decision boundary for some initial adversarial sample.
- We introduce an online learning technique to build prior knowledge from successful attacks. Through sequential attacks, a group of prominent initial adversarial images are organized into 2 levels of class-specific and global dictionaries to be used as candidate initial adversarial samples for upcoming attacks. We empirically demonstrate that the top-1 entry of the global dictionary is one of the *universal* adversarial images and establish theoretical properties for such images. Exploiting the prior information significantly reduces the average queries.

## II. RELATED WORKS

The black-box attack scenarios can be categorized based on the attacker’s knowledge. The Transfer-based attacks rely on the transferability of adversarial examples among models and exploit substitute models to craft them like attacks proposed in [44], [20], [31], [37]. In this scenario the attacker has access to the data distribution but has no information about the model. Another category is score-based attack that limits the attacker knowledge only to the model scores such as the class probabilities or logits. The attacker tries to estimate the gradient of the model from the score through significant number of queries. [6], [35], [40], [52], [16], [42], [3], [32] are some of the efficient methods in this group. Decision-based attacks are the most challenging scenario which narrows the the attackers vision only to the classifier’s top-1 hard label output. The first work considering decision-based attack was the Boundary Attack (BA) proposed in [8]. BA estimates the boundary and moves along it to minimize the perturbation. The Query-Limited Attack [32] leverages a Monte-Carlo approximation approach to approximate the model scores based on the label-setting only and from there on, proceeds with score-based Partial Information Attack as presented earlier.

Another efficient decision-based method is HopSkipJumpAttack (HJSA) [15] which is based on estimating the gradient direction using top-1 class labels. A natural evolutionary (NE) algorithm has been introduced to update the data covariance matrix after certain queries to reduce the search space from a sphere to an quadratic eclipse characterized by the covariance matrix. A similar approach in updating covariance matrix based on truncated Gaussian distributions is leveraged to adapt Deepfool to the decision-based GeoDA method [46]. Natural evolutionary strategies (NES) were first considered by Ilyas, et. al. [32] in designing query-efficient attacks.

Cheng, et. al. [18] model the top-1 label attack as a real-valued optimization problem and use zeroth-order optimization approach to design query-efficient attack using randomized gradient-free method (RGF). Zhao, et. al. [58] have proposed ZO-ADMM method where they integrate the alternating direction method of multipliers (ADMM) with zeroth-order (ZO) optimization and Bayesian optimization (BO) to design a

query-efficient gradient-free attack. In [19], the authors extend the optimization based approach and estimate the gradient sign at any direction instead of the gradient itself and introduce Sign-OPT which is more query-efficient compared to OPT.

Another sign-based method, SIGN-HUNTER [2] exploits a sign-based gradient approximation rather than magnitude-based to devise a binary black-box optimization. Their method does not rely on hyper-parameter tuning or dimensionality reduction. Chen, et. al. have suggested to randomly flip the signs of a small number of entries in adversarial perturbations and this way, boost the attacker’s performance, specifically in defensive models compared to EA, BA, SignOPT, and HSJA [17]. [9] offers a bias for gradient direction based on a surrogate model. RaySearch is another recent approach [14] which advantages over HJSA, and Sign-OPT in efficiency. RaySearch proceeds by finding the closest decision boundary via solving a discrete optimization problem that does not require any zeroth-order gradient estimation. Dimension reduction based attack techniques are investigated to achieve query efficiency. Sign-OPT-FFT[19], Bayes Attack [49], SimBA-DCT[28], QEBA-S, QEBA-F, QEBA-I, and GeoDA-Subspace[46] are which are effective in  $\ell_2$  attacks, but in order to guarantee other imperceptibility bounds, they must fetch to the original and transformation domains consecutively, imposing computational burden on their procedure. Certain methods focus on crafting attacks which are sparse in the image original dimensions such as SparseFool [39], GreedyFool [23], Sparse attack via perturbation factorization [25] (for white-box), and Sparse-RS [22], CornerSearch [21] and GeoDA (sparse version) [46] (for black-box).

## III. PROPOSED METHOD: LSDAT

The proposed LSDAT method is considered for untargeted black-box adversarial attack. Untargeted attack can be formulated as the following optimization problem:

$$\min_{\delta} \|\delta\|_p \quad s.t. \quad \mathcal{C}(\mathbf{X}_0 + \delta) \neq \mathcal{C}(\mathbf{X}_0), \quad (1)$$

where  $\delta$  denotes the added perturbation. The goal is to minimize the perturbation  $\ell_p$ -norm such that when applied to the input image  $x_0$ , the classifier  $\mathcal{C}$  is fooled.

Since LSD is one of the main building blocks of the proposed attack, here we briefly introduce it first to be self-contained. LSD is a well-established optimization problem studied in classical machine learning with image and video processing applications including video surveillance, object detection, background subtraction, text extraction, face reconstruction, and manifold learning [43], [7], [59], [36], [5]. LSD is an image-agnostic and non-data-driven transform which assumes most images can be explained with a low-rank background plus a sparse part. Mathematically, if the image to be perturbed is denoted by  $\mathbf{X}$ , LSD can be formalized as:

$$\min_{\mathbf{L}, \mathbf{S}} \text{rank}(\mathbf{L}) + \lambda \|\mathbf{S}\|_0, \quad s.t. \quad \mathbf{X} = \mathbf{L} + \mathbf{S}, \quad (2)$$

where  $\mathbf{L}$  is the low rank and  $\mathbf{S}$  is the sparse component. The regularization coefficient  $\lambda$  determines the sparsity level of  $\mathbf{S}$ . The convex surrogate functions for the rank function and the

$\ell_0$ -norm are considered to be the trace norm  $\|\cdot\|_*$  and the  $\ell_1$ -norm, respectively. Hence, Problem (2) can be cast as a convex optimization problem

$$\min_{\mathbf{L}, \mathbf{S}} \|\mathbf{L}\|_* + \lambda \|\mathbf{S}\|_1, \quad \text{s.t. } \mathbf{X} = \mathbf{L} + \mathbf{S}. \quad (3)$$

The sparse part consists of far less (in terms of order of magnitude) pixels compared to the original image dimensions; while these reduced data are highly informative and well represent details of the image and are therefore decisive in classification [57], [56], [55].

Algorithm 1 summarizes the proposed LSDAT. An initial adversarial sample (with a ground truth label different from the original image) is randomly selected. LSD is performed on the original and the adversarial images. Next, the sparse components of the two images  $\mathbf{S}_o$  and  $\mathbf{S}_a$  are considered. The union of non-zero pixels in the sparse components form a low-dimensional subspace  $\mathcal{S}$  in the original domain. There are noticeably fewer coordinates in  $\mathcal{S}$  in order for crafting the perturbation which can significantly reduce the query number (which generally scale with the dimensions and why low-dimensional transforms are of interest). Narrowing down the attack vision to  $\mathcal{S}$ , we propound that for some certain initial adversarial sample  $\mathbf{X}_a$ , the perturbation direction  $\mathbf{S}_a - \mathbf{S}_o$  is the most aligned sparse direction with the shortest path ( $\delta$ ) from  $\mathbf{X}_o$  to the decision boundary. This will be theoretically shown in Section V.

---

#### Algorithm 1 LSDAT with one initial adversarial sample

---

**Require:**  $(\mathbf{X}_o, r)$ : Original image and its class,  $\mathbf{X}_a$ : Initial adversarial sample,  $\text{MaxIter}$ : Maximum number of iterations,  $\alpha$ : sparse traversing rate,  $p$ :  $\ell_p$  constraint type,  $\mathcal{T}$  = Imperceptibility constraint budget  $\{k, \epsilon, \sigma\}$   
**Output:**  $\mathbf{X}_p$ : Perturbed image,  $N_Q$ : Number attempted queries,  $F_{\text{attack}}$ : Attack success flag  
**Initialization:**  $\mathbf{X}_p \leftarrow \mathbf{0}$ ,  $N_Q \leftarrow 0$ ,  $F_{\text{attack}} \leftarrow \text{False}$ ,  $i \leftarrow 1$   
1:  $(\mathbf{L}_o, \mathbf{S}_o) \leftarrow \text{LSD}(\mathbf{X}_o)$ ,  $(\mathbf{L}_a, \mathbf{S}_a) \leftarrow \text{LSD}(\mathbf{X}_a)$   
2: **while**  $i \leq \text{MaxIter}$  **do**  
3:    $\mathbf{S}_i \leftarrow (\alpha \times i)\mathbf{S}_a + (1 - \alpha \times i)\mathbf{S}_o$   
4:    $\mathbf{S}_i \leftarrow \mathbf{S}_o + \Pi_p(\mathbf{S}_i - \mathbf{S}_o, \mathcal{T})$   
5:    $\mathbf{X}_i \leftarrow \mathbf{L}_o + \mathbf{S}_i$   
6:    $c = \text{Query}(\mathbf{X}_i)$   
7:   **if**  $c \neq r$  **then**  
8:      $F_{\text{attack}} \leftarrow \text{True}$ ,  $N_Q \leftarrow i$ ,  $\mathbf{X}_p \leftarrow \mathbf{X}_i$   
9:     **break**  
10:   **end if**  
11:    $i = i + 1$   
12: **end while**  
13: **return**  $\mathbf{X}_p, N_Q, F_{\text{attack}}$

---

The attack attempts to induce a new sparse pattern ( $\mathbf{S}_a$ ) into this  $\mathbf{X}_p$  which is highly informative of  $\mathbf{X}_a$  and suppresses  $\mathbf{S}_o$  while traversing from  $\mathbf{S}_o$  to  $\mathbf{S}_a$ . It is worth noting that the alteration from one sparse component to another is done via a weighted combination of both. Since the traversing is in a low-dimensional subspace, the semantic transform from  $\mathbf{X}_o$  to  $\mathbf{X}_a$  is carried out rapidly and within few steps (queries). In other words, small step sizes (perturbations) in the sparse domain leads to more drastic changes in the image concept. In Section V, we will show how a locally linear classifier (LLC) functions well based on a basis of low rank and sparse components and verify the efficacy of using sparse components

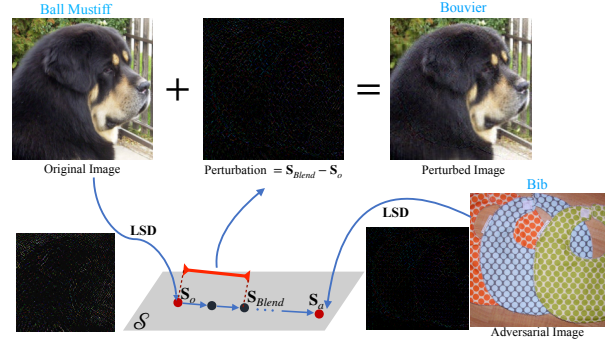


Fig. 2: Illustration of LSDAT. Perturbation lies on the path  $\mathbf{S}_a - \mathbf{S}_o$  and is added in a step-wise fashion to  $\mathbf{S}_o$ , which is finally added to  $\mathbf{X}_o$ .

as decisive elements in classification. Fig. 2 demonstrates this procedure.

After obtaining the perturbation on the specified direction of  $\mathbf{S}_a - \mathbf{S}_o$ , it is added to the low-rank component  $\mathbf{L}_o$  to form the candidate perturbed image for each query. One motivation of preferring LSD to FFT-based methods is that although transform methods like FFT-based or spatial-based approaches optimally represent geometric structure information of images, they cannot extract entire contours and edges accurately, while the LSD can extract the edges and salient parts of an image in an image-agnostic fashion. Side effects, such as pseudo Gibbs phenomenon and false contours are downsides of domain transform-based methods [56].

To satisfy the imperceptibility constraints in the LSDAT procedure, after obtaining the perturbation  $\mathbf{S}_a - \mathbf{S}_o$ , it is projected on the  $\ell_p$ -ball depending on the imperceptibility constraint. Projection is denoted by  $\Pi_p$  in Alg. 1 line 4. we apply appropriate projections depending on the type of imperceptibility constraint ( $\ell_p$  norm) denoted with operation  $\Pi$  in Alg. 1 line 6.

#### A. LSDAT with Imperceptibility Constraints

Adversarial attacks designed to be confined with certain imperceptibility constraints, to make them feasible, by limiting the norm of the perturbation.  $\ell_p$  norm bounds are the prevalent perturbation constraints considered in the literature. In our work, we consider  $\ell_0$ ,  $\ell_2$ , and  $\ell_\infty$  norm bounds on the perturbations.

## IV. CHALLENGE OF SELECTING INITIAL ADVERSARIAL SAMPLE

As stated previously, the perturbation direction of interest is set as  $\mathbf{S}_a - \mathbf{S}_o$  for some random  $\mathbf{S}_a$  to maintain sparsity and small perturbation  $\ell_p$  norm. One random choice may not yield the optimal perturbation direction. Thanks to noticeable query-efficiency of LSDAT, we can explore among several initial adversarial samples. We call this set of random samples the *exploration* set,  $\mathcal{E}$ . If the initial adversarial image budget of an attack per sample is  $G$ , the set  $\mathcal{E}$  is gathered such that  $|\mathcal{E}| = G$ . To launch an attack to the image  $\mathbf{X}_o$ , we consider one sample at the time, drawn from  $\mathcal{E}$  as the initial adversarial sample and apply Alg. 1 to it. Figure 3 Note that, if the



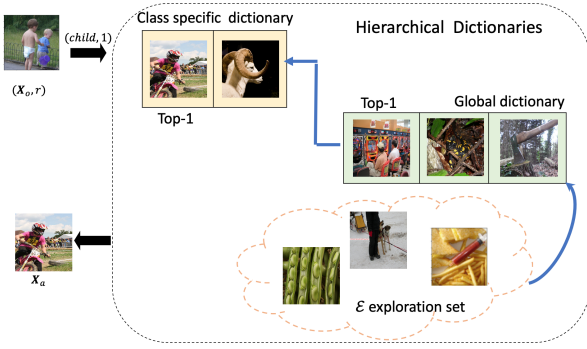


Fig. 3: Hierarchical dictionary structure for initial adversarial sample provider. At each point the sample is fetched based on the class label  $r$  and the index  $i$  in the the budget  $G$ .

attack is successful at any point, the rest of the exploration set will not be attempted. Thus, the number of queries is  $(j \times MaxIter) + N_Q$ , where  $j$  is the number of unsuccessful initial adversarial attempts and  $N_Q$  is the number of queries used in the successful attack.

#### A. Online Learning with Hierarchical Dictionaries

Black-box attack scenarios can be categorized into isolated and non-isolated ones. In non-isolated attacks, where the goal is to attack a set of images rather than a single one, the attacker can build a prior knowledge through the attacking process by learning the set of elite samples which are universal in fooling the previously attacked input images. These prominent samples are organized into a hierarchy of *class-specific* and *global* dictionaries. The intuition is that if one sample serves as a good initial adversarial image for multiple images of a specific class; for instance the class cat; it is also very likely to be a good initial adversarial point for the other instances of that class. If the class specific dictionary does not have any entry or the number of entries is limited, the best initial adversarial points are those which have successfully fooled other classes so far. All dictionaries' entries are always ranked based on their score, which is defined as the number of successful attacks for that image as an initial adversarial image up to now. Our proposed dictionary-based attack exploits the previous good initial adversarial samples to launch a new attack with fewer queries. In a new attack on an image  $\mathbf{X}$  with label  $r$  and the initial adversarial image budget of  $G$ , first the entries of class-specific dictionary for class  $r$  are selected one after the other as the initial adversarial image. If none of them leads to an adversarial counterpart for  $\mathbf{X}_o$  and the budget  $G$  is not met, the remaining initial images are picked from the global dictionary and if exhausted, from random sampling (Figure 3). If the attack is successful, we update the dictionaries accordingly, i.e. update the score for the dictionaries entries or adding a new item to them. As the attacking process continues, the dictionaries become richer to the point that top-1 entry of the global dictionary contributes significantly in successful attacks, we refer to this sample as *universal* adversarial initial image. The properties of such images are investigated theoretically in the next section.

## V. THEORETICAL ANALYSIS

Now, we establish the theoretical analysis for LSDAT. First, it is worth noting that most of decision-based attack methods in the literature rely on estimating the decision boundary, the gradient, and in some instances the second derivative. Obtaining an estimation the aforementioned necessitates certain number of queries to the model, which contravenes the query-limited assumption. Our method is designed for extremely limited query regime. Thus, estimating the decision boundary or the gradient are avoided in LSDAT procedure and it is adapted for extremely low-query budgets. (In experimental section, we include "max-1" query attack results for LSDAT to manifest LSDAT functionality under extremely query-limited scenarios. This is despite the fact that most SOTA methods are dysfunctional for very limited budgets. We assume the original and the adversarial image are decomposed as  $\mathbf{X}_o = \mathbf{L}_o + \mathbf{S}_o$ ,  $\mathbf{X}_a = \mathbf{L}_a + \mathbf{S}_a$ , where  $\mathbf{L}_o, \mathbf{S}_o$  and  $\mathbf{L}_a, \mathbf{S}_a$  denote the low rank and sparse components of the original and the adversarial images, respectively. The goal is to show that  $\mathbf{S}_a - \mathbf{S}_o$  is a viable sparse perturbation centered around  $\mathbf{X}_o$  that can fool the model. Before delving into the analysis, we elaborate on the geometric interpretation of LSDAT functionality, as depicted in Fig. 4. It is known that an  $\ell_1$ -ball centered at  $\mathbf{X}_o$  has sharp corners (vertices). If one gradually enlarges congruent  $\ell_1$ -balls centered at  $\mathbf{X}_o$ , it is highly likely that one of them intersects the decision boundary at one of its sharp corners which is a well-known property of  $\ell_1$  contours. Certain  $\ell_1$ -balls centered at  $\mathbf{X}_o$  also intersect with the subspace spanned by  $\mathbf{S}_o$  and  $\mathbf{S}_a$  denoted as  $\mathcal{S}$ . The intersection can be formulated as  $\sum_i w_{1i} |s_{oi}| + \sum_j w_{2j} |s_{aj}| = cte$  where  $s_{oi}$  and  $s_{aj}$  are the  $i$  and  $j$  element of  $\mathbf{S}_o$  and  $\mathbf{S}_a$  respectively. A specific direction which lies on  $\mathcal{S}$  and also forms a vertex for one  $\ell_1$ -ball (due to sparsity is  $\mathbf{S}_a - \mathbf{S}_o$ ). The goal is to show that for some initial  $\mathbf{S}_a$ , traversing the path  $\mathbf{S}_a - \mathbf{S}_o$  starting from  $\mathbf{X}_o$  introduces a viable sparse perturbation which is highly likely to be the most aligned sparse direction with the shortest path to decision boundary ( $\delta$ ) compared to other vertices of the  $\ell_1$ -ball  $\|\mathbf{X} - \mathbf{X}_o\|_1 = cte$ . Therefore, it is both sparse and hence norm-constrained, and also likely to cross a decision boundary due to relative alignment with  $\delta$ . The described concept can be visually observed in Fig. 4. Now, we delve into mathematical analyses. First, we assume the decision boundary can be locally linearized in part of an  $\epsilon$ -net covered by  $\mathbf{X}_o$  and some initial  $\mathbf{X}_a$  in the exploration set  $\mathcal{E}$  (for larger  $\|\mathcal{E}\|$ , LSDAT is more likely to find such  $\epsilon$ -net), where  $\epsilon$  is a small value. In general, considering there are  $P$  nearest samples in an  $\epsilon$ -net covering local decision boundary, a locally linear classifier (LLC) can be estimated using regression on a basis composed of low-rank and sparse components  $\mathcal{B} = \{\mathbf{L}_i, \mathbf{S}_i\}_{i=1}^P$ . The local regression weights can be used for classification (fed to a linear SVM for instance).

It is shown in [57] that LLC trained on the basis formed by LSD components of nearest samples yield favorable classifier with small generalization error. An LLC is governed by certain regression weights near each sample. This leads to a nonlinear classifier in general as different parameters are to be utilized for different local regions. Considering an  $\epsilon$ -net covering

decision boundary consisting of  $\mathbf{X}_o$ , the desired LLC can be obtained as follows:

$$\min_{\mathbf{c}_p} \sum_{p=1}^P \|\mathbf{X}_p - \mathcal{B}\mathbf{c}_p\|^2 + \lambda \|\mathbf{d}_p \odot \mathbf{c}_p\|^2, \quad (4)$$

where  $\mathbf{d}_p$  is defined as  $\mathbf{d}_p = \exp(\frac{dist(\mathbf{X}_p, \mathcal{B})}{\sigma})$ .  $\sigma$  determines the decay rate for locality, and  $dist(\mathbf{X}_p, \mathcal{B})$  is the distance between  $\mathbf{X}_p$  and basis elements in  $\mathcal{B}$ . Therefore, any sample in this  $\epsilon$ -net can be written using the low rank and sparse basis expansion as

$$\mathbf{X}_p = \mathcal{B}\mathbf{c}_p = \bar{\mathcal{B}}(\epsilon)\bar{\mathbf{c}}_p + \mathcal{B}(\epsilon)\mathbf{t}, \quad (5)$$

where  $\mathcal{B}(\epsilon) = [\mathbf{L}_o, \mathbf{S}_o, \mathbf{L}_a, \mathbf{S}_a]$ ,  $\bar{\mathcal{B}}(\epsilon) = \mathcal{B} \setminus \mathcal{B}(\epsilon)$ , and  $\bar{\mathbf{c}}_p, \mathbf{t}$  are split components of  $\mathbf{c}_p$  indexing  $\bar{\mathcal{B}}(\epsilon)$  and  $\mathcal{B}(\epsilon)$ , respectively. The LLC prioritizes the components based on the distance from the samples. We have assumed the  $\epsilon$ -net is covered by  $\mathbf{X}_o$  and  $\mathbf{X}_a$ . Thus, they are dominant terms in LLC, and for some  $\tau(\epsilon, \sigma)$  which is increasing w.r.t  $\sigma$  and  $\epsilon$ ,  $\|\mathbf{t}\| > (1 - \tau(\epsilon, \sigma))\mathbf{c}_p$ . This means,

$$\|\mathbf{X}_p - \mathcal{B}(\epsilon)\mathbf{t}\| = \|\bar{\mathcal{B}}(\epsilon)\bar{\mathbf{c}}_p\| \leq \tau(\epsilon, \sigma)\|\bar{\mathcal{B}}(\epsilon)\|_{op}\|\bar{\mathbf{c}}_p\| \quad (6)$$

For small  $\sigma$  and  $\epsilon$  values,  $\tau$  becomes small and the dominant components of  $\mathbf{c}_p$  index  $\mathcal{B}(\epsilon)$ . Taking the latter into account,  $\mathbf{X}_p = \mathcal{B}(\epsilon)\mathbf{t} + \mathcal{O}(\tau) \approx \mathcal{B}(\epsilon)\mathbf{t}$ .

We are specifically interested in some point  $\mathbf{X}_p$  (as the perturbed image) that lies in the  $\epsilon$ -net and while maintaining the sparsest perturbation form  $\mathbf{X}_o$ , fools the model. Let  $\mathbf{t} = [t_1, t_2, t_3, t_4]$ . The perturbation  $\mathbf{X}_p - \mathbf{X}_o$  can be written as,

$$\mathcal{B}(\epsilon)\mathbf{t} = (t_1 - 1)\mathbf{L}_o + (t_2 - 1)\mathbf{S}_o + t_3\mathbf{L}_a + t_4\mathbf{S}_a \quad (7)$$

It is desired that the perturbation 1- be sparse (or  $\ell_p$  bounded) as much as possible, 2- be aligned with the side information fooling direction  $\mathbf{X}_a - \mathbf{X}_o$  as much as possible, and 3- the perturbed image  $\mathbf{X}_p$  be close to  $\mathbf{X}_a$  in the  $\epsilon$ -net as much as possible so as to cross the boundary and fool the model. Therefore, to find the desired perturbation, the following optimization over  $\mathbf{t}$  is suggested:

$$\begin{aligned} & \min_{[t_1, t_2, t_3, t_4]} \underbrace{\mu \|(t_1 - 1)\mathbf{L}_o + (t_2 - 1)\mathbf{S}_o + t_3\mathbf{L}_a + t_4\mathbf{S}_a\|_1}_{\text{sarsity measure}} + \\ & \lambda \theta \left( \underbrace{(t_1 - 1)\mathbf{L}_o + (t_2 - 1)\mathbf{S}_o + t_3\mathbf{L}_a + t_4\mathbf{S}_a, \mathbf{X}_a - \mathbf{X}_o}_{\text{alignment with the difference direction } \mathbf{L}_a + \mathbf{S}_a - \mathbf{L}_o - \mathbf{S}_o} \right) + \\ & \underbrace{\|(t_1 - 1)\mathbf{L}_o + (t_2 - 1)\mathbf{S}_o + t_3\mathbf{L}_a + t_4\mathbf{S}_a\|_2}_{\text{distance of } \mathbf{X}_p \text{ to the adversarial sample}} \end{aligned} \quad (8)$$

When  $\mu$  is large enough (which is a reasonable assumption enforcing restricted perturbation norm), coefficients of  $\mathbf{L}_o$  and  $\mathbf{L}_a$  tend to 0 in the  $\ell_1$  regularized term promoting sparsity because these are largely non-sparse terms compared to  $\mathbf{S}_o$  and  $\mathbf{S}_a$  (similar to sparse group lasso [50]). This leads to  $t_1 = 1, t_3 = 0$ . Therefore, the sparsity-constrained term shrinks to  $\|(t_2 - 1)\mathbf{S}_o + t_4\mathbf{S}_a\|_1$ . Assuming orthogonality of linear combination of  $\mathbf{S}_o$  and  $\mathbf{S}_a$  to  $\mathbf{L}_a - \mathbf{L}_o$ <sup>2</sup>, the third term (distance

of  $\mathbf{X}_p$  to  $\mathbf{X}_a$ ) can be written as  $\|t_1\mathbf{L}_o + (t_3 - 1)\mathbf{L}_a\|_2 + \|t_2\mathbf{S}_o + (t_4 - 1)\mathbf{S}_a\|_2$ . As stated,  $t_1$  and  $t_3$  values are forced by large  $\mu$ . The compromise between the controllable expression in the third term  $\|t_2\mathbf{S}_o + (t_4 - 1)\mathbf{S}_a\|_2$  and the sparsity regularizer, i.e.,  $\|t_2\mathbf{S}_o + (t_4 - 1)\mathbf{S}_a\|_2 + \mu\|(t_2 - 1)\mathbf{S}_o + t_4\mathbf{S}_a\|_1$  determines the blending (linear combination) weights in  $\mathcal{S}$ . The sparsity regularizer is minimized for  $t_2 = 1, t_4 = 0$  (trivial solution, and the  $\ell_2$  term minimization yields  $t_2 = 0, t_4 = 1$ . Therefore, when there is a compromise of both (large  $\mu < \infty$ ), the solutions lie somewhere on the sparse perturbation vector  $(\mathbf{0}, \mathbf{S}_a - \mathbf{S}_o)$ . The second term in loss function also works in favor of the  $\ell_2$  term, weighing the balance of solutions towards  $t_2 = 0, t_4 = 1$ . (It is worth noting that as  $\mu$  is large, the  $\ell_1$  term is dominant. Thus, solution path tends to a linear interpolator between  $(\mathbf{0}, \mathbf{S}_a - \mathbf{S}_o)$ .) It is worth noting that as the  $\epsilon$ -net setting may not be realized and therefore the basis expansion on sparse components and the aforementioned optimization is not valid. This may lead to larger perturbation norm to cross decision boundary corresponding to other classes. The point is although the direction is not optimal (to save for numerous queries required to estimate the gradient and decision boundary, a sparse perturbation which is likely to align with it is introduced.), thanks to query-efficiency we can attempt many samples from  $\mathcal{E}$  as far as the query budget allows. This gives rise to the probability of crossing some decision boundary even if the adversarial sample is not optimal via LSDAT procedure. Moreover, the perturbation may cross another decision boundary before crossing the desired one which is in this case favorable to the method's performance, making LSDAT suitable for untargeted attack.

As mentioned, there may exists some universal samples in a dictionary of elite samples which are globally capable of fooling the model for input samples from diverse classes. Although the path  $\mathbf{S}_a - \mathbf{S}_o$  has been shown to be the most aligned (best sparse approximation) sparse direction with  $\delta$ , yet this alignment can vary depending on existence of the  $\epsilon$ -net and the angle between  $\delta$  and  $\mathbf{S}_a - \mathbf{S}_o$ . The angle depends on how sparse the  $\delta$  is itself. Theoretically, they are universally most aligned if  $\delta$  is close to its sparse approximation  $\mathbf{S}_a - \mathbf{S}_o$  as much as possible. As stated before,  $\delta$  is expressed in the basis  $\mathcal{B}(\epsilon)$  and will be the sparsest if in the representation  $(t_1 - 1)\mathbf{L}_o + (t_2 - 1)\mathbf{S}_o + t_3\mathbf{L}_a + t_4\mathbf{S}_a, t_3 = 0$  or to put it differently, the sample itself is almost its sparse component and its texture (low-rank component) is negligible or very small.

It is worth noting that although the method is designed for the sparse ( $\ell_1$ ) attack, as  $\ell_1$  and  $\ell_2$  norms of a vector are cohered, the  $\ell_2$  also is likely to shrink which makes LSDAT to be applicable for  $\ell_2$  attacks as well. Although, the presented sparse perturbation is not necessarily same as the minimal  $\ell_2$  distance to the decision boundary, the partial alignment contains information of the minimal perturbation

<sup>3\*\*\*</sup>As we care about sparse attack, we have only provided analysis for  $\ell_1$  loss on  $\delta$  in P(8). We have provided  $\ell_2$  and  $\ell_\infty$  attacks adapting the proposed sparse perturbation to other non  $\ell_1$  scenarios. One can interchangeably, adapt the first loss to  $\ell_2$  and include terms incorporating  $\mathbf{L}_o$  and  $\mathbf{L}_a$ . The reason we suffice to the sparse version is simplicity by traversing the proposed path in a sparse domain involving few pixels. \*\*\*

<sup>2</sup>This is a reasonable assumption on the basis  $\mathcal{B}$ .

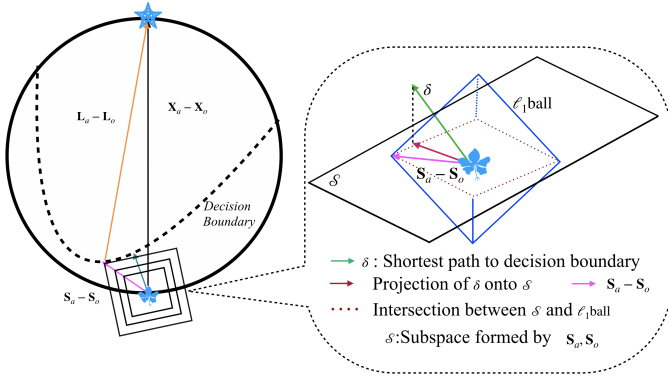


Fig. 4: Geometric illustration of LSDAT. The attempt is to show that among sparse directions,  $\mathbf{S}_a - \mathbf{S}_o$  is likely to be the most aligned one with the shortest path to decision boundary  $\delta$ , and therefore is likely to cross the decision boundary as well as maintaining perturbation norm efficiency.

and makes the sparse perturbation also likely to cross the decision boundary.

## VI. COMPLEXITY AND CONVERGENCE RATE ANALYSIS

A general fact is that the number of queries scale with the image dimensions as each coordinate can play a role in fooling the model. To remedy the curse of dimensionality in crafting adversarial perturbation for high-dimensional data, domain transforms are applied to the original image in order to design the perturbation in a low-dimensional space. FFT-based methods such as QEBA-F [35], Bayes-Attack [49] are the most query-efficient attack method to the best of our knowledge. Although reducing the required queries, performing low-dimensional transforms and their inverse impose extra computational burden per each query.

The complexity of the FFT-based methods (for  $m = n$ ) are dominated by  $\mathcal{O}(2N \times t \times n^2 \log_2(n))$ , where  $N$  is the number of queries,  $n$  denote original dimension,  $t$  is the iterations per query for FFT and its inverse IFFT. Although increasing the efficiency, such transforms come at the cost of increased query-wise complexity. Additionally, FFT-based methods do not obtain control on non- $\ell_2$  (such as  $\ell_0$  or  $\ell_\infty$ ) perturbation constraints in the transform domain. This mandates applying extra transforms to perform clipping, thresholding, and projections back in the original domain in order for satisfying such imperceptibility constraints. Extra transforms come at the cost of more computational burden. While LSDAT directly maneuvers the image in the original domain obtaining direct control on such constraints.

On the contrary, LSDAT merits over such methods as it only applies a one-time initial LSD for initial samples attempted from the exploration set. Next, it applies summations on sparse components in the original domain. As the sparse coding and the summation all happen in the original domain, there is no additional transform-related computational burden per query in LSDAT. The most efficient computational complexity corresponding to RPCA is obtained by accelerated alternating projections algorithm (IRCUR) [10] which is (for  $m = n$ )  $\mathcal{O}(Gnr^2 \log_2^2(n) \log_2(\frac{1}{\epsilon}))$ , where  $r$  is the rank of the low-rank component, and  $\epsilon$  is the accuracy of the low-rank component

(appearing as the number LSD solver algorithm iterations), and  $G$  is the number of explored samples in the exploration set  $\mathcal{E}$ . It immediately follows that the proposed are less complex compared to transform based methods with a factor of  $\frac{\log(n)}{n}$  which plays important role in high-dimensional setting.

Now, we provide convergence rate analysis for the proposed algorithm. Since the LSDAT attack relies on the weighted combination of sparse component of original image and that of adversarial image for fast semantic transform of the original image, and these sparse components are obtained at the early stage of the algorithm, the convergence rate only depends on how fast the weighted combination phase, sweeps the path between sparse components. Tuning the step size may not be a priority for  $\ell_0$  and  $\ell_\infty$  attacks as their perturbation metric does not depend on the distance swept between sparse parts. The choice of step-size, however, affects the perturbation norm for  $\ell_2$  constraint. Thus, the convergence rate of a successful attack only depends on the chosen step size. which can be set based on how much the perturbation budget. The convergence rate is then  $\frac{1}{\alpha}$ , where  $\alpha$  as also used in Alg. 1, is the modification rate between sparse parts. Large  $\alpha$ s lead to faster convergence.

## VII. EXPERIMENTAL SET-UP AND RESULTS

In this section, we present a comprehensive set of experiments to demonstrate the efficacy of the proposed LSDAT attack in degrading the performance of well-trained image classifiers for ImageNet. We apply LSDAT to attack two ImageNet pre-trained models<sup>4</sup>, namely ResNet-50 [29] and VGG16 [51] on the set  $\mathcal{D}$ , created by gathering correctly classified samples from the ImageNet validation set. We increase the step size in LSDAT implementations for  $\ell_0$  and  $\ell_\infty$  scenarios as it does not affect the corresponding constraints. Fast convergence of LSDAT with large step size allows us to expand the exploration set  $\mathcal{E}$  to increase the fooling rate. From now on, we abbreviate Average Queries and Fooling Rate with AQ and FR, respectively. In the following experiments, FR is defined based on the number of misclassified samples divided by the number of samples in  $\mathcal{D}$ . The reported number of queries is averaged on all successful attack instances. We compare the performance of LSDAT based on AQ, FR, and perturbation norm with state-of-the-art (SOTA) methods.

**LSDAT with  $\ell_2$  constraint:** For a fair comparison in  $\ell_2$  attack scenario, we use 1000 samples for the set  $\mathcal{D}$  and the initial adversarial samples budget is set to 100. For LSDAT(R), we select the initial samples randomly from validation set. Note that initial sample set varies for each image to be attacked. In LSDAT(D), we exploit the prior information by first selecting initial samples from the class specific (if exists) and then the global dictionary. If the initial adversarial sample budget is not met, the remaining samples are selected randomly. It is worth noting that we only add an image to the initial adversarial set, if the current images could not lead to a successful attack so far. The comparison of performance with the SOTA methods is presented in Table I. The LSDAT attack consistently outperforms all methods with a significant drop in AQ. LSDAT(R) leads to on average 28.7% and 29.6%

<sup>4</sup><https://pytorch.org/docs/stable/torchvision/models.html>



Method	Resnet-50						VGG-bn					
	$\epsilon = 5$		$\epsilon = 10$		$\epsilon = 20$		$\epsilon = 5$		$\epsilon = 10$		$\epsilon = 20$	
	FR	AQ	FR	AQ	FR	AQ	FR	AQ	FR	AQ	FR	AQ
BA[8]	8.52	666.5	15.39	577.9	26.97	538.1	11.23	626.3	21.27	547.6	39.37	503.2
OPT Attack[18]	7.64	777.4	15.84	737.2	32.53	757.9	11.09	736.6	21.79	658.9	43.86	718.7
HJSA[15]	6.99	904.3	14.76	887.1	28.37	876.8	10.30	893.2	21.53	898.2	40.82	892.6
Sign-OPT[19]	7.46	777.4	15.84	737.1	32.53	757.9	19.81	841.1	35.8	843.7	60.63	857.7
Bayes Attack[49]	20.10	64.2	37.15	64.1	66.67	54.97	24.04	69.8	43.46	76.5	71.99	48.9
LSDAT(R)	23.40	53.9	47.6	41.5	75.20	35.6	30.20	58.8	55.6	43.8	81.00	33.9
LSDAT(D)	<b>25.40</b>	<b>35.2</b>	<b>47.6</b>	<b>39.4</b>	<b>76.80</b>	<b>21.50</b>	<b>32.80</b>	<b>36.4</b>	<b>56.80</b>	<b>32.9</b>	<b>82.40</b>	<b>15.2</b>

TABLE I: Comparison of different  $\ell_2$  attack methods performance on ImageNet based on various  $\ell_2$  ball constraint  $\epsilon$  for Effect of hyper parameters ). FR and AQ stand for fooling rate and average query respectively. In LSDAT(x), x="R" represents random samples, x="D" stands for Dictionary base. Best performances are in bold.

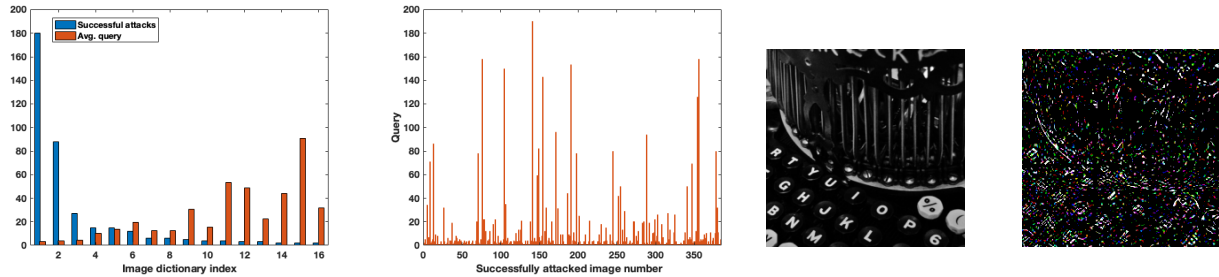


Fig. 5: From left to right,(1) Successful attacks (blue bars) and average query distribution of global dictionary samples with success rate  $> 1$ . The orange bar represents the average query per successful attack. (2) The number of queries for each successful attack. (3) The top-1 image of the global dictionary. (4) The sparse component of the top-1 image which is scaled for the sake of visibility.

Method	ResNet-50		VGG16-bn	
	FR	AQ	FR	AQ
OPT Attack[18]	5.73	246.3	7.53	251.2
Sign-OPT[19]	10.31	660.4	15.85	666.6
Bayes Attack[49]	67.48	45.9	<b>78.47</b>	<b>33.7</b>
LSDAT(R)	<b>70.00</b>	31.3	76.20	43.2
LSDAT(D)	69.40	<b>29.4</b>	74.80	37.3

TABLE II: Comparison of performance of LSDAT  $L_\infty$  attack for  $\sigma = 0.05$  with STOA methods.

reduction in AQ while it improves the fooling rate by 17.38% and 31.16% for ResNet-50 and VGG models, respectively compared to Bayes attack[49]. Applying LSDAT(D), the attack further improves the FR while reducing the AQ by 47.6% for Resnet-50 and 57% for VGG compared to Bayes attack. The AQ gain is one order of magnitude compared to other methods.

**Universal Adversarial Sparse Image:** We also analyze the effectiveness of dictionary in reducing the AQ and finding the universal adversarial sparse image. To this end we apply LSDAT(D) attack with  $\ell_2$  constraint of  $\epsilon = 20$  on a set with  $|\mathcal{D}| = 500$ . The initial sample budget is 100 with  $MaxIter=2$  per sample. This setting leads to 384 successful attacks. Figure 5-left shows the distribution of dictionary samples that bring about at least 2 successful attacks in blue bars along with the AQ per attack for each image in orange bars. Manifestly, the top-1 image in the global dictionary gives rise to 46.8% of successful attacks with as low as 3.27 query per attack and the top-5 samples are responsible for 86.7% of successes with average of 7.11 query per attack. These findings support

the existence of a universal sample with a sparse component whose difference to the input sparse component is highly likely to align with the shortest path from  $\mathbf{X}_o$  to the decision boundary ( $\delta$ ). The top-1 image and its sparse component are illustrated in the last 2 images of Figure 5 respectively. Clearly, the sparse component contains most of the details including keys while the background(texture) is black.

**LSDAT with  $\ell_\infty$  or  $\ell_0$  constraint:** In case of  $\ell_\infty$  attack, the attack setting is the same as  $\ell_2$  constrained attack. Table II summarizes the performance comparison of LSDAT with SOTA methods when the  $\ell_\infty$  perturbation bound is  $\sigma = 0.05$ . The proposed attack, consistently outperforms all methods for ResNet-50 architecture while it achieves similar results as the runner-up method for the VGG16-bn architecture. We believe the lower performance on VGG16-bn roots in the ability of the model in extracting richer features by considering both local and global spatial information, compared to ResNet which makes the attack more difficult.

Finally, we compare LSDAT attack in  $\ell_0$  scenario with GeoDA [46] in Table III. GeoDA achieves the best FR with limited query budget compared to other sparse attacks such as Sparse-RS [21], [22]. Also, Bayes Attack [49] is not the first choice to apply for  $\ell_0$  constraint as it suits  $\ell_2$  and the sparsity level is less controllable in frequency domain due to FFT transformation mandating computational burden and further queries. To have a fair comparison with GeoDA, the set  $\mathcal{D}$  contains 500 samples with the initial adversarial sample budget  $G = 100$ . Both, LSDAT(R) and LSDAT(D) significantly outperform GeoDA and improve the AQ by at least one order of magnitude. Also, the superiority of LSDAT is clear in

P%	Method					
	GeoDA[46]		LSDAT(R)		LSDAT(R)	
	FR	AQ	FR	AQ	FR	AQ
4.29	88.44	500	85.20	12.6	<b>90.00</b>	<b>8.3</b>
3.05	82.30	500	80.20	15.3	<b>83.40</b>	<b>8.6</b>
2.36	75.20	500	76.80	15.3	<b>80.10</b>	<b>10.0</b>
1.00	47.00	500	60.60	17.6	<b>64.00</b>	<b>12.2</b>
0.50	30.00	500	49.80	24.2	<b>51.20</b>	<b>17.2</b>

TABLE III: Comparison of LSDAT  $\ell_0$  attack performance to Resnet-50 model under various perturbation rates (P%) with GeoDA. In LSDAT(x), x="R" represents random initial adversarial samples, x="D" stands for Dictionary base.

highly imperceptible  $\ell_0$  attacks when only 0.5% – 1% of coordinates are perturbed. FR is improved up to 21.2% and 17% by perturbing only 0.5% and 1% coordinates respectively, setting the state-of-the-art performance for the imperceptible  $\ell_0$  attacks.

**Attacking Adversarially Robust Models:** We also evaluate the effectiveness of LSDAT against adversarially robust models. To this end, we consider the method proposed by [54] for fast adversarial training that leads to a robust Resnet-50 classifier on ImageNet with 43% robust accuracy on PGD attacks. The result of comparison of LSDAT with GeoDA with various perturbation rate for  $\ell_0$  constraint attacks are reported in Table IV. While LSDAT(x) achieve higher FR with significantly lower AQ compared to GeoDA, we noticed that LSDAT(R) slightly outperforms LSDAT(D) in terms of FR. This phenomena is expected as the adversarial training changes the shape of decision boundary and makes the dictionary entries with small score less reliable as an inertial adversarial images. This necessitates finding a balance factor between exploration set and exploiting dictionary. We postpone this study to our future works.

**Pure Black-Box Attack:** The most challenging type of black-box attacks is known as pure black box attack in which *only one query* is allowed to launch an attack. We evaluated the performance of the LSDAT in this scenario. LSDAT(R) achieves FR of 25.8% and 33.6% on Resnet-50 and VGG respectively for  $\ell_2$  constraint of  $\epsilon = 20$ . With *only* 1% perturbation on  $\ell_0$  constraint attacks, the FR=24.4% for Resnet and FR=21% for VGG can be obtained. Finally on  $\ell_\infty$  attack with constraint of  $\sigma = 0.05$  the FR is 26% and 25.4% on ResNet and VGG, respectively. Note that other decision-based black box attacks are not applicable in this threat models as they demand more than one query to estimate the decision boundary. For instance, GeoDA[46] requires at least 10 queries to obtain average  $\ell_2$  distance of 39.4 which is as twice as LSDAT with a single query.

### VIII. CONCLUDING REMARKS

A query-efficient decision-based adversarial attack (LSDAT) is introduced based on low-rank and sparse decomposition. The method is suitable for very limited query budgets and is of low complexity compared to SOTA. LSDAT is also effective in fooling rate dominating the SOTA in performance as verified through diverse set of experiments. LSDAT finds a sparse perturbation which is likely to be aligned with the sparse

P%	Method					
	GeoDA[46]		LSDAT(R)		LSDAT(D)	
	FR	AQ	FR	AQ	FR	AQ
4.29	71.30	500	73.00	19.71	<b>73.00</b>	<b>9.8</b>
3.05	60.10	500	<b>65.00</b>	20.3	62.20	<b>13.1</b>
2.36	54.70	500	<b>60.00</b>	24.0	58.10	<b>10.8</b>
1.00	36.80	500	<b>44.00</b>	27.2	43.00	<b>18.7</b>
0.50	22.60	500	<b>30.00</b>	32.2	26.20	<b>21.1</b>

TABLE IV: Comparison of LSDAT  $\ell_0$  attack performance to an adversarially robust Resnet-50 model under various perturbation rates (P%) with GeoDA. In LSDAT(x), x="R" represents random initial adversarial samples, x="D" stands for Dictionary base.

approximation of the shortest path from input sample to the decision boundary. We show the path lies on the path connecting original and some adversarial sparse components. Theoretical analyses buttresses LSDAT performance in fooling. Moreover, LSDAT offers better control over imperceptibility constraints in the original domain and less complexity compared to SOTA as it does not apply consecutive transforms and their inverse. Experiments on the well-known ImageNet dataset shows query efficiency and fooling rate superiority of LSDAT compared to SOTA.

### REFERENCES

- [1] Naveed Akhtar and Ajmal Mian. Threat of adversarial attacks on deep learning in computer vision: A survey. *IEEE Access*, 6:14410–14430, 2018. 1
- [2] Abdullah Al-Dujaili and Una-May O’Reilly. Sign bits are all you need for black-box attacks. In *International Conference on Learning Representations*, 2019. 2
- [3] Moustafa Alzantot, Yash Sharma, Supriyo Chakraborty, Huan Zhang, Cho-Jui Hsieh, and Mani B Srivastava. Genattack: Practical black-box attacks with gradient-free optimization. In *Proceedings of the Genetic and Evolutionary Computation Conference*, pages 1111–1119, 2019. 2
- [4] Anish Athalye, Logan Engstrom, Andrew Ilyas, and Kevin Kwok. Synthesizing robust adversarial examples. In *International conference on machine learning*, pages 284–293. PMLR, 2018. 1
- [5] Masoumeh Azghani, Ashkan Esmaili, Kayhan Behdin, and Farokh Marvasti. Missing low-rank and sparse decomposition based on smoothed nuclear norm. *IEEE Transactions on Circuits and Systems for Video Technology*, 30(6):1550–1558, 2019. 2
- [6] Arjun Nitin Bhagoji, Warren He, Bo Li, and Dawn Song. Practical black-box attacks on deep neural networks using efficient query mechanisms. In *European Conference on Computer Vision*, pages 158–174. Springer, 2018. 2
- [7] Thierry Bouwmans, Necdet Serhat Aybat, and El-hadi Zahzah. *Handbook of robust low-rank and sparse matrix decomposition: Applications in image and video processing*. CRC Press, 2016. 2
- [8] Wieland Brendel, Jonas Rauber, and Matthias Bethge. Decision-based adversarial attacks: Reliable attacks against black-box machine learning models. *arXiv preprint arXiv:1712.04248*, 2017. 2, 7
- [9] Thomas Brunner, Frederik Diehl, Michael Truong Le, and Alois Knoll. Guessing smart: Biased sampling for efficient black-box adversarial attacks. In *Proceedings of the IEEE International Conference on Computer Vision*, pages 4958–4966, 2019. 2
- [10] HanQin Cai, Keaton Hamm, Longxiu Huang, Jiaqi Li, and Tao Wang. Rapid robust principal component analysis: Cur accelerated inexact low rank estimation. *IEEE Signal Processing Letters*, 2020. 6
- [11] Nicholas Carlini, Pratyush Mishra, Tavish Vaidya, Yuankai Zhang, Micah Sherr, Clay Shields, David Wagner, and Wenchao Zhou. Hidden voice commands. In *25th {USENIX} Security Symposium ({USENIX} Security 16)*, pages 513–530, 2016. 1
- [12] Nicholas Carlini and David Wagner. Towards evaluating the robustness of neural networks. In *2017 IEEE Symposium on Security and Privacy (SP)*, pages 39–57. IEEE, 2017. 1
- [13] Nicholas Carlini and David Wagner. Audio adversarial examples: Targeted attacks on speech-to-text. In *2018 IEEE Security and Privacy Workshops (SPW)*, pages 1–7. IEEE, 2018. 1



- [14] Jinghui Chen and Quanquan Gu. Rays: A ray searching method for hard-label adversarial attack. In *Proceedings of the 26th ACM SIGKDD International Conference on Knowledge Discovery & Data Mining*, pages 1739–1747, 2020. 2
- [15] Jianbo Chen, Michael I Jordan, and Martin J Wainwright. Hop-skipjumpattack: A query-efficient decision-based attack. In *2020 IEEE Symposium on Security and Privacy (SP)*, pages 1277–1294. IEEE, 2020. 2, 7
- [16] Pin-Yu Chen, Huan Zhang, Yash Sharma, Jinfeng Yi, and Cho-Jui Hsieh. Zoo: Zeroth order optimization based black-box attacks to deep neural networks without training substitute models. In *Proceedings of the 10th ACM Workshop on Artificial Intelligence and Security*, pages 15–26, 2017. 2
- [17] Weilun Chen, Zhaoxiang Zhang, Xiaolin Hu, and Baoyuan Wu. Boosting decision-based black-box adversarial attacks with random sign flip. In *Proceedings of the European Conference on Computer Vision*, 2020. 2
- [18] Minhao Cheng, Thong Le, Pin-Yu Chen, Jinfeng Yi, Huan Zhang, and Cho-Jui Hsieh. Query-efficient hard-label black-box attack: An optimization-based approach. *arXiv preprint arXiv:1807.04457*, 2018. 2, 7
- [19] Minhao Cheng, Simranjit Singh, Patrick Chen, Pin-Yu Chen, Sijia Liu, and Cho-Jui Hsieh. Sign-opt: A query-efficient hard-label adversarial attack. *arXiv preprint arXiv:1909.10773*, 2019. 2, 7
- [20] Shuyu Cheng, Yinpeng Dong, Tianyu Pang, Hang Su, and Jun Zhu. Improving black-box adversarial attacks with a transfer-based prior. In *Advances in Neural Information Processing Systems*, pages 10934–10944, 2019. 2
- [21] Francesco Croce, Maksym Andriushchenko, Naman D Singh, Nicolas Flammarion, and Matthias Hein. Sparse-rs: a versatile framework for query-efficient sparse black-box adversarial attacks. *arXiv preprint arXiv:2006.12834*, 2020. 2, 7
- [22] Francesco Croce and Matthias Hein. Sparse and imperceivable adversarial attacks. In *Proceedings of the IEEE International Conference on Computer Vision*, pages 4724–4732, 2019. 2, 7
- [23] Xiaoyi Dong, Dongdong Chen, Jianmin Bao, Chuan Qin, Lu Yuan, Weiming Zhang, Nenghai Yu, and Dong Chen. Greedyfool: Distortion-aware sparse adversarial attack. *arXiv preprint arXiv:2010.13773*, 2020. 2
- [24] Kevin Eykholt, Ivan Evtimov, Earlene Fernandes, Bo Li, Amir Rahmati, Chaowei Xiao, Atul Prakash, Tadayoshi Kohno, and Dawn Song. Robust physical-world attacks on deep learning visual classification. In *Proceedings of the IEEE Conference on Computer Vision and Pattern Recognition*, pages 1625–1634, 2018. 1
- [25] Yanbo Fan, Baoyuan Wu, Tuanhui Li, Yong Zhang, Mingyang Li, Zhifeng Li, and Yujiu Yang. Sparse adversarial attack via perturbation factorization. In *Proceedings of European Conference on Computer Vision*, 2020. 2
- [26] Ian J Goodfellow, Jonathon Shlens, and Christian Szegedy. Explaining and harnessing adversarial examples. *arXiv preprint arXiv:1412.6572*, 2014. 1
- [27] Kathrin Grosse, Nicolas Papernot, Praveen Manoharan, Michael Backes, and Patrick McDaniel. Adversarial perturbations against deep neural networks for malware classification. *arXiv preprint arXiv:1606.04435*, 2016. 1
- [28] Chuan Guo, Jacob R Gardner, Yurong You, Andrew Gordon Wilson, and Kilian Q Weinberger. Simple black-box adversarial attacks. *arXiv preprint arXiv:1905.07121*, 2019. 2
- [29] Kaiming He, Xiangyu Zhang, Shaoqing Ren, and Jian Sun. Deep residual learning for image recognition. In *Proceedings of the IEEE conference on computer vision and pattern recognition*, pages 770–778, 2016. 6
- [30] Weiwei Hu and Ying Tan. Black-box attacks against rnn based malware detection algorithms. *arXiv preprint arXiv:1705.08131*, 2017. 1
- [31] Zhichao Huang and Tong Zhang. Black-box adversarial attack with transferable model-based embedding. *arXiv preprint arXiv:1911.07140*, 2019. 2
- [32] Andrew Ilyas, Logan Engstrom, Anish Athalye, and Jessy Lin. Black-box adversarial attacks with limited queries and information. *arXiv preprint arXiv:1804.08598*, 2018. 2
- [33] Andrew Ilyas, Logan Engstrom, and Aleksander Madry. Prior convictions: Black-box adversarial attacks with bandits and priors. *arXiv preprint arXiv:1807.07978*, 2018. 1
- [34] Alexey Kurakin, Ian Goodfellow, and Samy Bengio. Adversarial examples in the physical world. *arXiv preprint arXiv:1607.02533*, 2016. 1
- [35] Huichen Li, Xiaojun Xu, Xiaolu Zhang, Shuang Yang, and Bo Li. Qeba: Query-efficient boundary-based blackbox attack. In *Proceedings of the IEEE/CVF Conference on Computer Vision and Pattern Recognition*, pages 1221–1230, 2020. 2, 6
- [36] Xin Liu, Guoying Zhao, Jiawen Yao, and Chun Qi. Background subtraction based on low-rank and structured sparse decomposition. *IEEE Transactions on Image Processing*, 24(8):2502–2514, 2015. 2
- [37] Yanpei Liu, Xinyun Chen, Chang Liu, and Dawn Song. Delving into transferable adversarial examples and black-box attacks. *arXiv preprint arXiv:1611.02770*, 2016. 2
- [38] Aleksander Madry, Aleksandar Makelov, Ludwig Schmidt, Dimitris Tsipras, and Adrian Vladu. Towards deep learning models resistant to adversarial attacks. *arXiv preprint arXiv:1706.06083*, 2017. 1
- [39] Apostolos Modas, Seyed-Mohsen Moosavi-Dezfooli, and Pascal Frossard. Sparsefool: a few pixels make a big difference. In *Proceedings of the IEEE Conference on Computer Vision and Pattern Recognition*, pages 9087–9096, 2019. 2
- [40] Hadi Mohaghegh Dolatabadi, Sarah Erfani, and Christopher Leckie. Advflow: Inconspicuous black-box adversarial attacks using normalizing flows. *Advances in Neural Information Processing Systems*, 33, 2020. 2
- [41] Seyed-Mohsen Moosavi-Dezfooli, Alhussein Fawzi, and Pascal Frossard. Deepfool: a simple and accurate method to fool deep neural networks. In *Proceedings of the IEEE conference on computer vision and pattern recognition*, pages 2574–2582, 2016. 1
- [42] Nina Narodytska and Shiva Kasiviswanathan. Simple black-box adversarial attacks on deep neural networks. In *2017 IEEE Conference on Computer Vision and Pattern Recognition Workshops (CVPRW)*, pages 1310–1318. IEEE, 2017. 2
- [43] Ricardo Otazo, Emmanuel Candes, and Daniel K Sodickson. Low-rank plus sparse matrix decomposition for accelerated dynamic mri with separation of background and dynamic components. *Magnetic resonance in medicine*, 73(3):1125–1136, 2015. 2
- [44] Nicolas Papernot, Patrick McDaniel, Ian Goodfellow, Somesh Jha, Z Berkay Celik, and Ananthram Swami. Practical black-box attacks against machine learning. In *Proceedings of the 2017 ACM conference on computer and communications security*, pages 506–519, 2017. 2
- [45] Nicolas Papernot, Patrick McDaniel, Somesh Jha, Matt Fredrikson, Z Berkay Celik, and Ananthram Swami. The limitations of deep learning in adversarial settings. In *2016 IEEE European symposium on security and privacy (EuroS&P)*, pages 372–387. IEEE, 2016. 1
- [46] Ali Rahmati, Seyed-Mohsen Moosavi-Dezfooli, Pascal Frossard, and Huaiyu Dai. Geoda: a geometric framework for black-box adversarial attacks. In *Proceedings of the IEEE/CVF Conference on Computer Vision and Pattern Recognition*, pages 8446–8455, 2020. 2, 7, 8
- [47] Waseem Rawat and Zenghui Wang. Deep convolutional neural networks for image classification: A comprehensive review. *Neural computation*, 29(9):2352–2449, 2017. 1
- [48] Mahmood Sharif, Sruti Bhagavatula, Lujo Bauer, and Michael K Reiter. Adversarial generative nets: Neural network attacks on state-of-the-art face recognition. *arXiv preprint arXiv:1801.00349*, 2(3), 2017. 1
- [49] Satya Narayan Shukla, Anit Kumar Sahu, Devin Willmott, and J Zico Kolter. Hard label black-box adversarial attacks in low query budget regimes. *arXiv preprint arXiv:2007.07210*, 2020. 2, 6, 7
- [50] Noah Simon, Jerome Friedman, Trevor Hastie, and Robert Tibshirani. A sparse-group lasso. *Journal of computational and graphical statistics*, 22(2):231–245, 2013. 5
- [51] Karen Simonyan and Andrew Zisserman. Very deep convolutional networks for large-scale image recognition. *arXiv preprint arXiv:1409.1556*, 2014. 6
- [52] Chun-Chen Tu, Paishun Ting, Pin-Yu Chen, Sijia Liu, Huan Zhang, Jinfeng Yi, Cho-Jui Hsieh, and Shin-Ming Cheng. Autozoom: Autoencoder-based zeroth order optimization method for attacking black-box neural networks. In *Proceedings of the AAAI Conference on Artificial Intelligence*, volume 33, pages 742–749, 2019. 2
- [53] Yevgeniy Vorobeychik and Murat Kantarcioglu. Adversarial machine learning. *Synthesis Lectures on Artificial Intelligence and Machine Learning*, 12(3):1–169, 2018. 1
- [54] Eric Wong, Leslie Rice, and J Zico Kolter. Fast is better than free: Revisiting adversarial training. *arXiv preprint arXiv:2001.03994*, 2020. 8
- [55] John Wright, Allen Y Yang, Arvind Ganesh, S Shankar Sastry, and Yi Ma. Robust face recognition via sparse representation. *IEEE transactions on pattern analysis and machine intelligence*, 31(2):210–227, 2008. 3
- [56] Baohua Zhang, Xiaoqi Lu, Haiquan Pei, Yanxian Liu, Wentao Zhou, and Doudou Jiao. Multi-focus image fusion based on sparse decomposition and background detection. *Digital Signal Processing*, 58:50–63, 2016. 3
- [57] Chunjie Zhang, Jing Liu, Qi Tian, Changsheng Xu, Hanqing Lu, and Songde Ma. Image classification by non-negative sparse coding, low-rank and sparse decomposition. In *CVPR 2011*, pages 1673–1680. IEEE,

2011. [3](#), [4](#)
- [58] Pu Zhao, Sijia Liu, Pin-Yu Chen, Nghia Hoang, Kaidi Xu, Bhavya Kailkhura, and Xue Lin. On the design of black-box adversarial examples by leveraging gradient-free optimization and operator splitting method. In *Proceedings of the IEEE International Conference on Computer Vision*, pages 121–130, 2019. [2](#)
- [59] Tianyi Zhou and Dacheng Tao. Godec: Randomized low-rank & sparse matrix decomposition in noisy case. In *Proceedings of the 28th International Conference on Machine Learning, ICML 2011*, 2011. [2](#)